

Revolutionizing $f(Q)$ Gravity Studies: Observational Cosmology through Deep Learning and Bayesian Analysis

Lokesh Kumar Sharma,^a Suresh Parekh,^b Anil Kumar Yadav,^c

^aDepartment of Physics, GLA University, Mathura 281406, India

^bDepartment of Physics, SP Pune University, Pune 411007, Maharashtra, India

^cDepartment of Physics, United College of Engineering and Research, Greater Noida 201310, India

E-mail: lokesh.sharma@gla.ac.in, thesureshparekh@gmail.com,
abanilyadav@yahoo.co.in

Abstract: One of the most exciting elements of cosmology is researching the potential of anisotropy in the early cosmos. We examine the expansion of the cosmos over time using an anisotropic Bianchi type-I spacetime subjected to the $f(Q)$ gravity. We do this by limiting the number of cosmological parameters used. The approach, we used is known as CoLFI, which stands for "Estimating Cosmological Parameters with deep learning." This paper presents a revolutionary deep learning-based technique to the parameter inference. The deep learning methodology clearly outperforms the MCMC method in terms of best-fit values, parameter errors, and correlations between parameters. This is the result of comparing the two different ways. Moreover, we obtained the transition redshift $z_t = 0.63$ which leads the transitioning model of the Universe from early deceleration to current acceleration phase. The dynamics of jerk parameter and validation of energy conditions of the model are also discussed.

Keywords: Cosmology; Machine Learning; Bayesian Method; large-scale structure of the Universe; $f(Q)$ gravity;

Contents

1	Introduction	2
2	Basic $f(Q)$ formalism	4
3	The Model	6
3.1	When $C = \gamma = 1$	7
3.2	When $C = 1, \gamma = 2$	7
3.3	When $C = 1, \gamma = 3$	8
4	Observational constraints	8
4.1	Bayesian Analysis	9
4.1.1	Artificial Neural Networks	11
4.1.2	Mixture Density Network	12
4.1.3	Mixture Neural Network	12
5	Physical parameters of the model	14
5.0.1	The pressure and the density of the energy	14
5.0.2	Equation of state parameter	16
5.0.3	Deceleration parameter	16
5.0.4	Statefinder analysis	17
5.0.5	Energy Conditions	18
5.1	Jerk Parameter	19
6	Concluding remarks	20

1 Introduction

An observer's point of view in space is not limited by his physical position or the direction in which he looks, according to cosmological principle. This highly useful assumption leads to a complete description of the modern Universe as a Friedmann Robertson-Walker (FRW) spacetime metric, which is basically isotropic and homogenous. However, such may not have been the case in the distant past or in the early phases of the Universe. Recent Wilkinson Microwave Anisotropy Probe (WMAP) findings [1–3] show that the basic isotropic and homogeneous model of the Universe has to be modified to fit observable data. Observations indicate that the inflationary paradigm [4] isotropizes the early Universe into today's FLRW geometry. To have a comprehensive understanding, it is still necessary to consider the probability of spatial anisotropy and inhomogeneity and then explore how this contributed to the observed levels of homogeneity and isotropy. While symmetries in the universe could exist, empirical evidences contradict this, including the small magnitude of the CMB quadrupole [5] and the low anomalies in the large scale angular distribution of the CMB power spectrum [6]. Alternative approaches to resolve the ongoing conflicts in the conventional Λ CDM model are highlighted by recent developments in cosmological research. The incredible constraining power of merging BAO and BBN data [7, 8] in their independent determination of the Hubble parameter H_0 [9]. This discovery was made possible without using cosmic microwave background data and revealed a notable 3.7σ tension with local distance ladder measurements. This collaboration between BAO and BBN probes provides a strong verification of Λ CDM predictions by connecting early and late-universe physics. In a study by Jimenez et al. (2023), photometric data and neural networks were used to predict $H(z)$ using cosmic chronometers, with a 10% accuracy rate [10]. Their research demonstrates the increasing importance of machine learning algorithms in cosmological parameter extraction from models with little model reliance, opening the door to new approaches to resolve differences in expansion rate observations. In order to better comprehend the dynamics of the Universe, these investigations highlight the urgent need for new frameworks that combine machine learning with other cosmological probes.

Various investigations, including $f(R, T)$ and $f(R)$ theories of gravity have also been carried out utilizing the modified theories of gravity (MTGs) [11–16]. Various areas of Bianchi cosmology have lately been investigated using observational data [17–19]. A lot of work has been done so far utilising the LRS-BI metric to investigate different parts of anisotropic cos-

mology in classical GR. According to Ref. [20], the LRS-BI metric has been used in GR theory to study the relationship between the jerk parameter and the ellipsoidal Universe, as well as the deceleration parameter and cosmic shear. Reference [21] is another book that contains Braneworld cosmology research on the ellipsoidal Universe. In 2011, L. Campanellie et al. examined the isotropy of the Universe utilizing type Ia supernovae data within the LRS-BI framework.[22] This study focuses on the LRS-BI model, which examines cosmic anisotropy through the application of a constant deceleration parameter for perfect fluids, alongside the concept of dynamically anisotropic dark energy. This study examines the LRS BI metric's anisotropic cosmological model within the framework of $f(R, T)$ gravity, incorporating a variable deceleration parameter. Furthermore, in Ref. [23], the de-Sitter and bounce solutions within $f(R, T)$ cosmology for the LRS-BI Universe have been examined. Recent efforts in $f(Q)$ gravity theory have also addressed anisotropic cosmology using the LRS BI metric. The energy density, equation of state, and skewness parameters are some of the cosmological profiles examined in $f(Q)$ gravity via the use of the LRS-BI metric that presents further results about the anisotropic Universe under $f(Q)$ gravity [24, 25]. Numerous numerical and statistical approaches are available in cosmology to explore complex models and interpret large amounts of observational data in $f(Q)$ gravity [26]. Despite expanding evidence, researchers seek improved data analysis methods to establish conclusions and optimize computer resources due to unsolved issues concerning physical reasons. In recent decades, machine learning and deep learning have offered alternatives to conventional data analysis approaches. Many tasks, such as classification, regression, image processing, and time series, have been successfully completed utilizing artificial neural networks (ANNs) [27]. They have advanced numerical calculations [28–30], model-independent reconstructions (nonlinear regression) [31–34], and object classification [30, 34–36]. However, most studies design the network architecture by generating a grid with several hyperparameter combinations and choosing the best. This may be computationally costly, and empirical architecture can provide inaccurate conclusions. Two problems plague ANNs despite their many benefits. Artificial networks feature dozens or millions of parameters (weights), making interpretation difficult. ANNs need careful selection of hyperparameters (e.g., number of layers, nodes, activation function, batch size) for accurate predictions. It is important to note that although certain neural network combinations might provide accurate predictions, others can lead to inaccurate physical interpretations in cosmology. Proper hyperparameter configuration ensures a balanced bias-variance neural model, preventing overfitting or underfitting [37]. This leads to reliable predictions and minimizes the weak interpretation of

multiple weights.

This is the paper's outline: We provide an overview of $f(Q)$ gravity using BI Universe in Section 2. Furthermore, we limited the model-free parameters in Section 4 using a Markov Chain Monte Carlo (MCMC) method and a deep learning approach using 55 observations from the OHD, BAO, and Pantheon SN Ia data compilations. Energy density, isotropic pressure, the EOS parameter, and energy conditions were all studied in Chapter IV. The consideration of findings and reasons brings Section 6 to a close.

2 Basic $f(Q)$ formalism

The action for $f(Q)$ is represented as [39]

$$S = \int \left[-\frac{1}{2}f(Q) + L_m \right] d^4x \sqrt{-g}, \quad (2.1)$$

In the equation $g_{\mu\nu}$, g is the determinant, $f(Q)$ is the non-metricity function, and L_m is the matter Lagrangian. Rearranging the variables (S) in the previous equation in relation to the metric causes the field equations to change.

$$\frac{2}{\sqrt{-g}} \nabla_\gamma (\sqrt{-g} f_Q P^{\gamma}_{\mu\nu}) + \frac{1}{2} f g_{\mu\nu} + f_Q (P_{\mu\gamma i} Q_v^{\gamma i} - 2Q_{\gamma i \mu} P^{\gamma i}_{\nu}) = T_{\mu\nu}, \quad (2.2)$$

where $f_Q = \frac{df}{dQ}$.

The range of variance concerning the connection is presented as

$$\nabla_\mu \nabla_\gamma (\sqrt{-g} f_Q P^{\gamma}_{\mu\nu}) = 0. \quad (2.3)$$

The Bianchi type I space-time can be interpreted as

$$ds^2 = -dt^2 + A^2(t)dx^2 + B^2(t)dy^2 + C^2(t)dz^2, \quad (2.4)$$

The scale factors along the x , y , and z axes are represented by the symbols $A(t)$, $B(t)$, and $C(t)$, respectively. The formula for calculating the average scale factor is represented as $a = (ABC)^{\frac{1}{3}}$.

Thus, the Hubble parameter of $A(t)$, $B(t)$ & $C(t)$ is defined as

$$H = \frac{1}{3} \left(\frac{\dot{A}}{A} + \frac{\dot{B}}{B} + \frac{\dot{C}}{C} \right). \quad (2.5)$$

Non-metricity is considered to be represented by the tensor of

$$Q = 6H^2. \quad (2.6)$$

Assuming a perfect fluid, the stress-energy tensor is obtained as

$$T_{\mu\nu} = (\rho + p) u_\mu u_\nu + p g_{\mu\nu}, \quad (2.7)$$

In this particular system, the symbol ρ is used to denote the energy density, p is used to represent the isotropic pressure, and $u_\mu u^\mu = -1$ for the four-velocity component.

The Friedmann equations for gravity are obtained by using the equation of motion (2.2) and the stress-energy tensor (2.7) in the Bianchi type model (2.4).

$$\frac{\dot{A}\dot{B}}{AB} + \frac{\dot{B}\dot{C}}{BC} + \frac{\dot{C}\dot{A}}{CA} = \frac{1}{2f_Q} \left(\rho + \frac{f}{2} \right), \quad (2.8)$$

$$\frac{\ddot{B}}{B} + \frac{\ddot{C}}{C} + \frac{\dot{B}\dot{C}}{BC} + \frac{1}{3} \frac{\dot{f}_Q}{f_Q} \left(\frac{\dot{A}}{A} + \frac{\dot{B}}{B} + \frac{\dot{C}}{C} \right) = \frac{1}{2f_Q} \left(-p + \frac{f}{2} \right), \quad (2.9)$$

$$\frac{\ddot{C}}{C} + \frac{\ddot{A}}{A} + \frac{\dot{A}\dot{C}}{AC} + \frac{1}{3} \frac{\dot{f}_Q}{f_Q} \left(\frac{\dot{A}}{A} + \frac{\dot{B}}{B} + \frac{\dot{C}}{C} \right) = \frac{1}{2f_Q} \left(-p + \frac{f}{2} \right), \quad (2.10)$$

$$\frac{\ddot{A}}{A} + \frac{\ddot{B}}{B} + \frac{\dot{A}\dot{B}}{AB} + \frac{1}{3} \frac{\dot{f}_Q}{f_Q} \left(\frac{\dot{A}}{A} + \frac{\dot{B}}{B} + \frac{\dot{C}}{C} \right) = \frac{1}{2f_Q} \left(-p + \frac{f}{2} \right), \quad (2.11)$$

the overdot symbolizes the derivative with regard to the time variable t .

Solving Eqs. (2.9) - (2.11), we obtain the following system of equations

$$\frac{\ddot{A}}{A} - \frac{\ddot{B}}{B} + \frac{\dot{A}\dot{C}}{AC} - \frac{\dot{B}\dot{C}}{BC} = 0 \quad (2.12)$$

$$\frac{\ddot{B}}{B} - \frac{\ddot{C}}{C} + \frac{\dot{A}\dot{B}}{AB} - \frac{\dot{A}\dot{C}}{AC} = 0 \quad (2.13)$$

$$\frac{\ddot{C}}{C} - \frac{\ddot{A}}{A} + \frac{\dot{B}\dot{C}}{BC} - \frac{\dot{A}\dot{B}}{AB} = 0 \quad (2.14)$$

Solving Eqs. (2.12) - (2.14), we obtain

$$\frac{\dot{B}}{B} + \frac{\dot{C}}{C} - 2\frac{\dot{A}}{A} = \frac{\kappa}{ABC}. \quad (2.15)$$

In this case, κ is an integration constant. Equation (2.15) does not often have an explicit solution that is practical. Nevertheless, a specific solution may be obtained when $\kappa = 0$. The following outcome is produced by solving equation (2.15) when $\kappa = 0$:

$$A^2 = BC \Rightarrow B = Ad \quad \& \quad C = \frac{A}{d} \quad (2.16)$$

The equation $d = d(t)$ represents the cosmic anisotropy.

The equations (2.16) and (2.5) provide the following outcome when combined:

$$H = \frac{\dot{A}}{A} \quad (2.17)$$

By applying Eq. (2.16) to any of Eqs. (2.9) - (2.11) and Eq. (2.8), we get

$$2\frac{\ddot{A}}{A} + \frac{\dot{A}^2}{A^2} + \frac{d^2}{d^2} + \frac{1}{3}\frac{\dot{f}_Q}{f_Q} \left(\frac{\dot{A}}{A} + \frac{\dot{B}}{B} + \frac{\dot{C}}{C} \right) = \frac{1}{2f_Q} \left(-p + \frac{f}{2} \right), \quad (2.18)$$

$$3\frac{\dot{A}^2}{A^2} - \frac{d^2}{d^2} = \frac{1}{2f_Q} \left(\rho + \frac{f}{2} \right), \quad (2.19)$$

The result is obtained by subtracting Equation (2.9) from Equation (2.11) and subsequently integrating the outcome.

$$\frac{\dot{A}}{A} - \frac{\dot{B}}{B} = \frac{k}{ABC} = \frac{k}{A^3} \quad (2.20)$$

The letter k represents the integration constant.

Using Eq. (2.16) in Eq. (2.20), we get

$$\frac{d^2}{d^2} = \frac{k^2}{A^6} \quad (2.21)$$

To ascertain the exact system solutions, it is necessary to constrain the scaling factor (a) or the deceleration parameter (q), as delineated in the equations. The subsequent section on cosmographic solutions will address this constraint.

In this work, we imitate $f(Q)$ gravity by use of a new fundamental Hubble parameterization in the shape

$$H = H_0(1+z)^{1+q_0-q_1} e^{q_1 z} \quad (2.22)$$

q_0 and q_1 are deceleration parameters of the derived universe model, where H_0 is the present Hubble constant.

3 The Model

A well-specified form of $f(Q)$ is required in order to derive the cosmological parameters. Without this, the examination of the cosmological model cannot proceed [39] have used the Pade's approximation to compute a numerical reconstruction of the cosmic observable up to massive red shifts. Typical cosmographic approaches are often plagued by convergence issues, however this provides an efficient method for defining cosmic observables up to huge red shifts. A numerical inversion method is used in order to restore $f(Q)$ by means of the equation $f(Q) = 6H^2$. Given these numerical data, the analytical function that best fits them is

$$f(Q) = CQ^\gamma \quad (3.1)$$

In the early universe, the acceleration phase is controlled by the actual value $\gamma > 1$, even though C and γ are free parameters of the model. This is because the expansion of the cosmos enters its acceleration phase at a later time. Numerous $f(Q)$ models have the same background development as the Λ CDM. However, we can measure the cosmic observable with great precision, and each of these theories impacts it uniquely.

3.1 When $C = \gamma = 1$

You may go back to the previously outlined ideas by following the same background development as in General Relativity.

The $f(Q)$ gravity is given by;

$$f(Q) = 6H^2 \quad (3.2)$$

therefore, the equations for ρ , p , and ω may be expressed as;

$$\rho = 12e^{2q_1z} H_0^2 (1+z)^{2+2q_0-2q_1} \left(-\frac{1}{4} - k^2(1+z)^6 + 3e^{2q_1z} H_0^2 (1+z)^{2+2q_0-2q_1} \right) \quad (3.3)$$

$$p = -3e^{2q_1z} H_0^2 (1+z)^{2+2q_0-2q_1} (-1 + 4k(1+z)^3) + 12e^{4q_1z} H_0^4 (1+z)^{4+4q_0-4q_1} \times (5 + 8q_0 - 8q_1 + 8q_1(1+z)) \quad (3.4)$$

$$\omega = \frac{(\frac{1}{4} - k(1+z)^3 + e^{2q_1z} H_0^2 (1+z)^{2+2q_0-2q_1} (5 + 8q_0 - 8q_1 + 8q_1(1+z)))}{-(\frac{1}{4}) - k^2(1+z)^6 + 3e^{2q_1z} H_0^2 (1+z)^{2+2q_0-2q_1}} \quad (3.5)$$

See Figures 5 and 6 for the ρ , p , and ω plots for $\gamma = 1$.

3.2 When $C = 1, \gamma = 2$

For this case, the $f(Q)$ gravity is given by

$$f(Q) = 36H^4 \quad (3.6)$$

Therefore, the equations for ρ , p , and ω may be expressed as

$$\rho = 72e^{4q_1z} H_0^4 (1+z)^{(4+4q_0-4q_1)} (-(1/4) - k^2(1+z)^6 + 3e^{2q_1z} H_0^2 (1+z)^{(2+2q_0-2q_1)}) \quad (3.7)$$

$$p = -18e^{4q_1z} H_0^4 (1+z)^{4+4q_0-4q_1} [-5 - 4q_0 + 4q_1 + 4k(1+z)^3 - 4q_1(1+z) \log e] + 72e^{6q_1z} H_0^6 (1+z)^{6+6q_0-6q_1} [-1 + 2q_0 - 2q_1 + 2q_1(1+z) \log e] \quad (3.8)$$

$$\omega = \frac{\left(\frac{5}{4} + q_0 - q_1 - k(1+z)^3 + q_1(1+z) \log e + e^{2q_1z} H_0^2 (1+z)^{2+2q_0-2q_1} (-1 + 2q_0 - 2q_1 + 2q_1(1+z) \log e)\right)}{-\left(\frac{1}{4}\right) - k^2(1+z)^6 + 3e^{2q_1z} H_0^2 (1+z)^{2+2q_0-2q_1}} \quad (3.9)$$

See Figures 5 and 6 for the ρ , p , and ω plots for $\gamma = 2$.

3.3 When $C = 1$, $\gamma = 3$

For this case, the $f(Q)$ gravity is given by

$$f(Q) = 216H^6 \quad (3.10)$$

Consequently, the relevant ρ , p , and ω equations are obtained as follows:

$$\begin{aligned} \rho = & 432e^{6q_1z} H_0^6 (1+z)^{6+6q_0-6q_1} \left[-\frac{1}{4} - k^2(1+z)^6 + 3e^{2q_1z} H_0^2 \left(432(1 + (1+z)^{2n})^3 H_0^6 \left(-\frac{1}{4} - k^2(1+z)^6 \right) \right. \right. \\ & + 3e^{2q_1z} H_0^2 (432(1 + (1+z)^{2n})^3 H_0^6 \left(-\frac{1}{4} - k^2(1+z)^6 \right) + 3(1 + (1+z)^{2n}) H_0^2 \\ & \left. \left. \left(432(1 + (1+z)^{2n})^3 H_0^6 \left(-\frac{1}{4} - k^2(1+z)^6 \right) + 3(1 + (1+z)^{2n}) H_0^2 \right) (1+z)^{2+2q_0-2q_1} \right] \end{aligned} \quad (3.11)$$

$$\begin{aligned} p = & -108e^{6q_1z} H_0^6 (1+z)^{6+6q_0-6q_1} (-1 + 4k(1+z)^3) & + 72e^{4q_1z} H_0^4 (1+z)^{4+4q_0-4q_1} \\ & \times (1 + q_0 - q_1 + q_1(1+z)) & + 432e^{8q_1z} H_0^8 (1+z)^{8+8q_0-8q_1} \\ & \times (-1 + 2q_0 - 2q_1 + 2q_1(1+z)) \end{aligned} \quad (3.12)$$

$$\begin{aligned} \omega = & \frac{\frac{1}{4} - k(1+z)^3 + e^{-2q_1z} (1+z)^{-2-2q_0+2q_1} (1 + q_0 - q_1 + q_1(1+z))}{6H_0^2} \\ & + \frac{e^{2q_1z} H_0^2 (1+z)^{2+2q_0-2q_1} (-1 + 2q_0 - 2q_1 + 2q_1(1+z))}{-\frac{1}{4} - k^2(1+z)^6 + 3e^{2q_1z} H_0^2 (1+z)^{2+2q_0-2q_1}} \end{aligned} \quad (3.13)$$

Figures 5 and 6 show the ρ , p , and ω plots for $\gamma = 3$.

4 Observational constraints

Through the use of χ^2 -minimization, the primary objective of this part is to acquire the free parameter of the derived universe model from the observational analysis. Using the following approaches, we are able to determine the values of the model parameters q_0 , q_1 , and H_0 :

4.1 Bayesian Analysis

In the past few years, cosmological research has increasingly used Bayesian inference for parameter estimation and model comparison. We carefully select a diverse variety of datasets to define limits and identify the relevant model parameters. What follows is a description and identification of these limits.

H(z) dataset

The differential age technique of galaxies is often used to determine the Hubble parameter, $H(z)$. Through the use of the relation

$$H(z) = -\frac{1}{1+z} \frac{dz}{dt},$$

it becomes possible to estimate the value of $H(z)$ at a given redshift z . The term $\frac{dt}{dz}$ is derived from observations of massive, passively evolving galaxies, which serve as reliable Cosmic Chronometers (CC). In our investigation, we utilized a dataset of 31 CC measurements compiled in [40–43]. These data points play a pivotal role in our analysis as they provide estimates of $H(z)$ across a range of redshifts.

It should be noted that, in this analysis, the correlations between the data points were not explicitly accounted for; the measurements were treated as uncorrelated. This assumption aligns with the standard practice in similar studies. To determine the best-fit model parameters, we employed a chi-squared minimization approach defined as:

$$\chi_{H(z)}^2 = \sum_{i=1}^{31} \left(\frac{H(H_0, \alpha, z_i) - H_{\text{obs}}(z_i)}{\sigma(z_i)} \right)^2, \quad (4.1)$$

where i indexes the 31 data points corresponding to specific redshifts z_i . Here, $H(H_0, \alpha, z_i)$ represents the theoretical prediction for the Hubble parameter at redshift z_i , $H_{\text{obs}}(z_i)$ denotes the observed Hubble parameter, and $\sigma(z_i)$ is the associated observational uncertainty at that redshift.

Pantheon+ dataset

In order to understand the universe’s accelerating expansion, Type Ia Supernovae (SNe Ia) are crucial. Significant spectroscopic evidence from a number of important surveys lend credence to this occurrence. These surveys include the SuperNova Legacy Survey (SNLS), the Sloan Digital Sky Survey (SDSS), the Hubble Space Telescope (HST) survey, and Panoramic

Survey Telescope and Rapid Response System (Pan-STARRS1). Because of their remarkably uniform peak brightness, these supernovae serve as "standard candles," allowing accurate cosmic distances to be calculated. The Pantheon+ sample is the most extensive dataset to date, with 1048 observations of the distance modulus throughout a redshift range of $0.01 \leq z \leq 2.3$ [44].

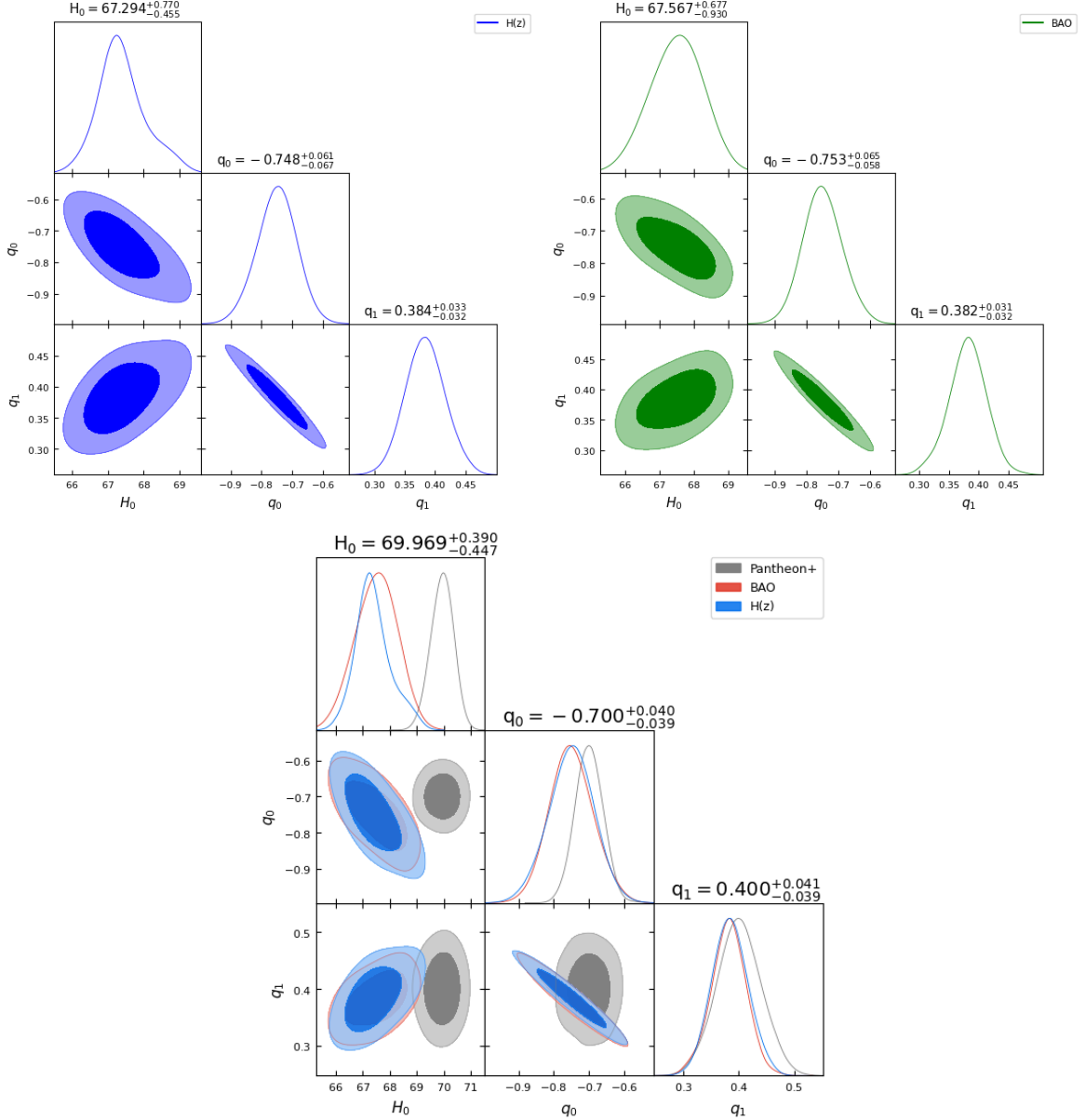


Figure 1: Two-dimensional contours at 1σ and 2σ confidence intervals are established by constraining our model using OHD, BAO, and *Pantheon*⁺ data.

To determine the best-fit model parameters, we compare theoretical predictions and observational measurements of the distance modulus, $\mu(z_k)$. Theoretically, the distance modulus is expressed as:

$$\mu_{\text{th}}(z_k) = \mu_0 + 5 \log_{10}(D_L(z_k)), \quad (4.2)$$

where the nuisance parameter μ_0 is given by:

$$\mu_0 = 25 + 5 \log_{10} \left(\frac{1}{H_0 \text{ Mpc}} \right), \quad (4.3)$$

and the luminosity distance $D_L(z)$ is defined as:

$$D_L(z) = (1+z) \int_0^z \frac{c d\xi}{H(\xi)}, \quad (4.4)$$

with c denoting the speed of light.

The χ^2 function for the Pantheon dataset, incorporating the covariance matrix C_{SNe} , is defined as:

$$\chi_{\text{Pan+}}^2(\mu_0, H_0, n) = \sum_{k,l=1}^{1048} \mu_k C_{\text{Pan+},kl}^{-1} \mu_l, \quad (4.5)$$

where $\mu_k = \mu_{\text{th}}(z_k, H_0, n) - \mu_{\text{obs}}(z_k)$. Here, $\mu_{\text{obs}}(z_k)$ represents the observed distance modulus, and $C_{\text{Pan+},kl}$ accounts for the covariance between the measurements.

The two-dimensional contours shown in Figure 1 reflect the 1σ and 2σ confidence zones, which are determined by using OHD to limit our model. The equation H_0 may be expressed as $km s^{-1} Mpc^{-1}$. In Table 1, you can see the predicted values of H_0 and q_0 .

Neural Networks

References [45–48] explain parameter estimation using ANN, MDN, and MNN. This study employs methods from Ref. [46] and the freely available code ColFI - <https://github.com/Guo-Jian-Wang/colfi> to estimate model parameters. The authors of Ref. [46] propose a mixed neural network (MNN) for parameter estimation, combining ANN and MDN. This can overcome both techniques' shortcomings.

4.1.1 Artificial Neural Networks

Artificial Neural Networks (ANNs) serve as a foundation for parameter estimation by mapping cosmological observations to parameter space. Figure 2 displays the H_0 , q_0 , and q_1 parameters with 1σ and 2σ confidence intervals obtained from the 57-point $H(z)$ dataset.

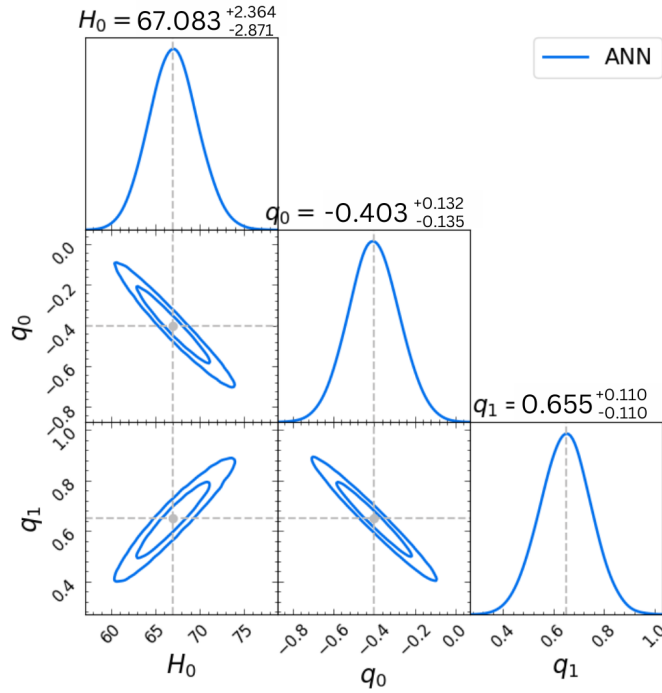


Figure 2: H_0 , q_0 , and q_1 1σ and 2σ contours from 57-point $H(z)$ data using ANN.

4.1.2 Mixture Density Network

Mixture Density Networks (MDNs) extend the ANN framework by modeling the parameter space probabilistically, effectively capturing uncertainties in parameter estimates. Figure 3 illustrates the resulting contour plots, showing the H_0 , q_0 , and q_1 parameters with corresponding confidence levels.

4.1.3 Mixture Neural Network

Mixture Neural Networks (MNNs) simplify the MDN methodology by directly estimating cosmological parameters using an ANN framework without explicit mixture models. This approach accelerates training while reducing instability. The results, shown in Figure 4, depict the H_0 , q_0 , and q_1 parameters with confidence contours derived from the same dataset.

The results produced by the ANN, MDN, and MNN methods to estimate the different parameters of the $f(Q)$ model are shown in Figs. 2, 3, and 4, respectively. Additionally, it should be noted that ColFi distinguishes itself from the MCMC technique by eschewing the use of likelihoods.

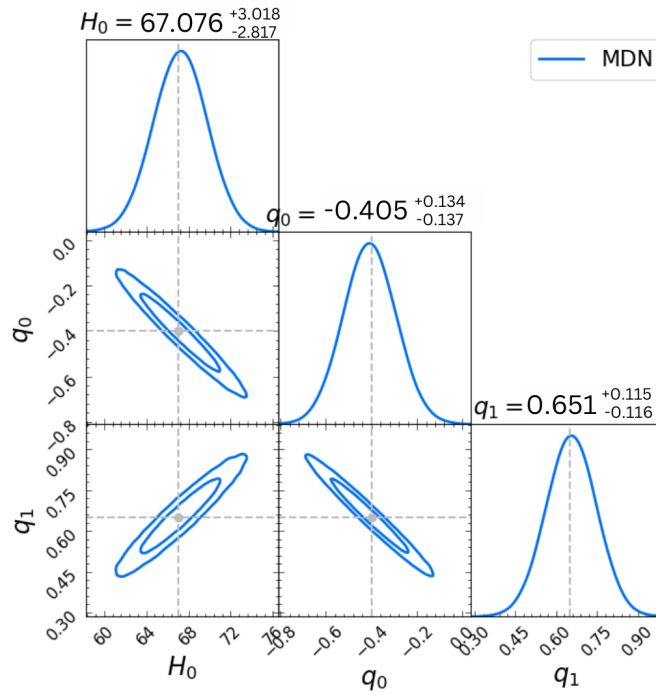


Figure 3: H_0 , q_0 , and q_1 1 σ and 2 σ contours from 57-point $H(z)$ data using MDN.

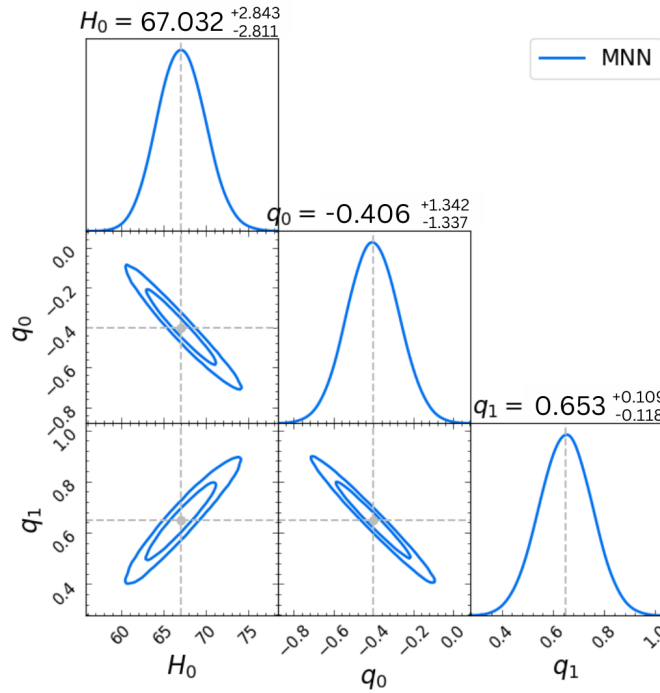


Figure 4: H_0 , q_0 , and q_1 1 σ and 2 σ contours from 57-point $H(z)$ data using MNN.

5 Physical parameters of the model

5.0.1 The pressure and the density of the energy

In this universe model, the energy density and pressure are calculated as

$$\rho = -2^{-1+\gamma} 3^\gamma (1+z)^{-2q_1} \times [e^{2q_1 z} H_0^2 (1+z)^{2+2q_0-2q_1}]^\gamma (-12e^{2q_1 z} H_0^2 (1+z)^{2+2q_0} + (1+z)^{2q_1}] \quad (5.1)$$

$$p = 2^{-1+\gamma} 3^\gamma (e^{2q_1 z} H_0^2 (1+z)^{2+2q_0-2q_1})^\gamma \times \left[1 - 12e^{2q_1 z} H_0^2 (1+z)^{2+2q_0-2q_1} + 4e^{2q_1 z} H_0^2 (1+z)^{2+2q_0-2q_1} \right. \\ \left. \times (1+q_0 - q_1 + q_1(1+z)) + 2^{4-\gamma} 3^{1-\gamma} e^{q_1 z} H_0 (1+z)^{1+q_0-q_1} \times \bar{p} \right] \quad (5.2)$$

where $\bar{p} = (e^{2q_1 z} H_0^2 (1+z)^{2+2q_0-2q_1})^{1-\gamma} (1+q_0 - q_1 + q_1(1+z))$. The generic form of the equation $f(Q) = cQ^\gamma$, which is the basis for the equations (5.1) and (5.0.1), demonstrates that the free parameters of the model are γ and c , both of which are equal to zero. The examination of certain values of γ might lead to the derivation of a specific form of $f(Q)$, which is an essential point to keep in mind. The form of gravity, denoted by the function $f(Q)$, is characterized as linear when γ is equal to one, as quadratic when γ is equal to two, and as cubic when γ is equal to three. Specifically, the figures 5 illustrate the progression of energy density ρ and pressure p in relation to redshift z for $\gamma = 1, 2$ & 3, respectively.

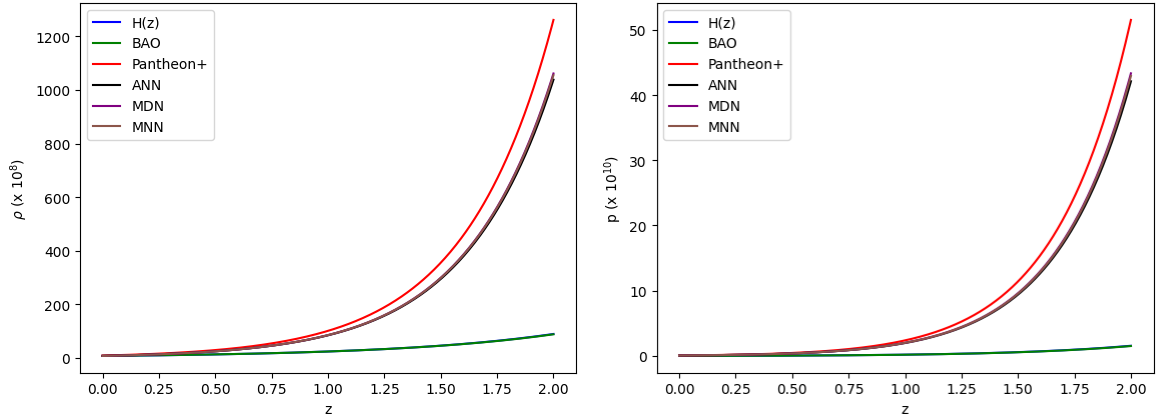


Figure 5: This plot displays the energy density ρ and pressure p vs the redshift z . On one side, we can see the density, and on the other, the pressure. Pressure p and energy density ρ are measured in GeV^4 and Pascal, respectively.

Figure 5 illustrates the evolution of the energy density ρ and pressure p in relation to the redshift z . Both the MCMC and NDEs methods show the variation of ρ with respect to z in the left panel of Figure 5, while the right panel shows the variation of p with respect to z . Around $z = 0$, we find a small positive value for the energy density, which decreases as z decreases. See the right panel of Figure 5 for the pressure-redshift connection. As z decreases, the cosmic pressure decreases as well.

For the purpose of providing an explanation for the late-time acceleration of the universe [49] that is caused by viscous fluid, Solanki and colleagues [50] conducted an investigation into a linear model in the field of $f(Q)$ gravity. In a subsequent research, Koussour and colleagues [51] conducted an investigation into this model by analyzing it with varying rates of geographical expansion. An investigation was conducted by the authors of the reference [52] to examine the quadratic form of gravity, which is represented by the function $f(Q)$. Additionally, the authors analyzed transitional events that were induced by a hybrid expansion rule. One of the most groundbreaking analyses of finite-time cosmological singularities and the potential future of the cosmos is offered in the reference [53]. An important research on the idea of gravity with a $f(Q)$ value may be found in the references [54–56]. Through this work, we have successfully reconstructed the $f(Q)$ theory of gravity by making the assumption that $f(Q) = cQ^\gamma$. This assumption leads to gravity that is linear, quadratic, cubic, and bi-quadratic, denoted by the function $f(Q)$. In contrast, the writers of the references [50–52] have investigated the linear and quadratic forms of the gravity function $f(Q)$. According to Solanki (2021), Koussour (2022), and Koussour (2022a), the gravity model that was generated uses the $f(Q)$ function, which is a generic model rather than an exiting defined model.

The left panel of Figure 5, which is a depiction of the model that is supplied in this work, displays the progression of the energy density ρ with redshift z . This is depicted in the figure. A tiny positive value is attained at the moment in time when the value of z is equal to zero, which is the same as the time that is now being experienced across the universe. Increasing the value of z results in a drop in the energy density, and at this point, it approaches a value that is relatively positive. A representation of the relationship between the change in pressure p and the change in redshift z is shown in the right panel of Figure 5 respectively. There is a detailed presentation of this volatility. The amount of pressure that the universe exerts begins to diminish at the same moment as the value of z begins to experience a reduction.

5.0.2 Equation of state parameter

Within the framework of the derived model, the equation of the state parameter ω may be found as

$$\omega = - \frac{(1+z)^{2q_1} \left(1 - 12e^{2q_1 z} H_0^2 (1+z)^{2+2q_0-2q_1} + \omega_1 \left(e^{2q_1 z} H_0^2 (1+z)^{2+2q_0-2q_1} \right)^{1-\gamma} (1+q_0 - q_1 + q_1(1+z)) \right)}{-12e^{2q_1 z} H_0^2 (1+z)^{2+2q_0} + (1+z)^{2q_1}} \quad (5.3)$$

where, $\omega_1 = 4e^{2q_1 z} H_0^2 (1+z)^{2+2q_0-2q_1} (1+q_0 - q_1 + q_1(1+z)) + 2^{4-\gamma} 3^{1-\gamma} e^{q_1 z} H_0 (1+z)^{1+q_0-q_1}$.

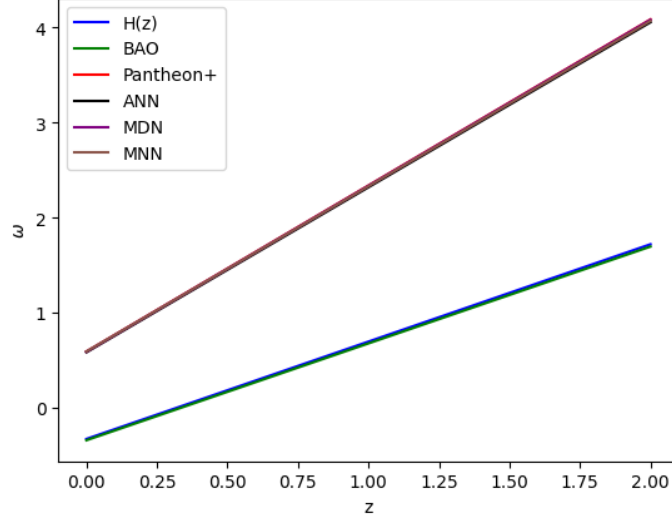


Figure 6: For $\gamma = 1, 2,$ and $3,$ the cubic $f(Q)$ gravity model's ω parameter's evolutionary behavior with respect to the redshift z was studied using Bayesian and Deep Learning statistics, respectively.

Figure 6 shows how the EOS parameter ω changes with redshift z . When ω is negative, it means the cosmos is expanding at a faster rate.

5.0.3 Deceleration parameter

As the deceleration parameter $q(z)$ evolves

$$q(z) = -1 + \frac{d}{dt} \left(\frac{1}{H} \right). \quad (5.4)$$

The variations mentioned in Eq. (2.22) help one to determine the variation in the deceleration parameter $q(z)$.

$$q(z) = q_0 - q_1 + q_1(1+z) \quad (5.5)$$

Figure 7 illustrates the transition from deceleration to acceleration along the z axis. Consistent with the findings presented in Refs. [57, 58], we calculate the phase transition values

of the transition redshift to be $z_t = 0.63$. Recent research has led authors to determine the transition redshift, yielding values of $z_t = 0.69^{+0.23}_{-0.12}$ [59] and $z_t = 0.60^{+0.21}_{-0.12}$ [60] and $z_t = 0.723^{+0.34}_{-0.16}$ [61]. The restricted value of z_t identified in this work aligns closely with the findings presented in Ref. [60].

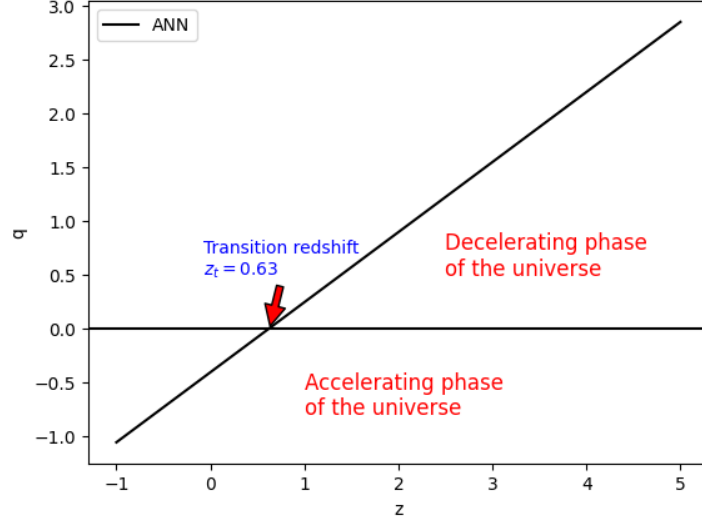


Figure 7: The illustration elucidates the relationship between $q(z)$ and the redshift z .

As seen in Figure 7, the universe goes through a decelerating phase when the redshift is greater than or equal to z_t , and an accelerating phase when the redshift is less than or equal to z_t . Because $\frac{dH}{dt} = 0$ and $q = -1$ at $z = -1$, the universe is expanding at its fastest pace. In addition, we calculated that $q_0 = -0.3527$ is the present-day DP value, which shows that the universe is expanding at a faster pace than it was in the past. References [61, 62] provide some pertinent constraints on the deceleration parameter.

5.0.4 Statefinder analysis

To distinguish Dark Energy (DE) models, state finder parameters (r, s) are read as

$$r = q(z) + 2q^2(z) - H^{-1}\dot{q}, \quad (5.6)$$

$$s = \frac{(r-1)}{3(q-1/2)}. \quad (5.7)$$

To illustrate the various DE models, consider the following examples: $((r = 1, s = 0))$, where $(r > 1, s < 0)$, where $(r < 1, s > 0)$ address the Λ CDM model, the CG model, and the quintessence model in that sequence.

Considering Equations (2.22), (5.6), (5.7), and (5.4), we can derive the pair of statefinder parameters (r, s) as

$$r = \frac{e^{-q_1 z} (1+z)^{-1-q_0} (q_0 - q_1 + q_1(1+z)) \left(-(1+z)^{q_1} + e^{q_1 z} H_0 (1+z)^{1+q_0} (1+2q_0 - 2q_1 + 2q_1(1+z)) \right)}{H_0} \quad (5.8)$$

$$s = \frac{2}{3} \left(1 + q_0 - q_1 + q_1 + q_1 z + \frac{e^{-q_1 z} (1+z)^{-1-q_0+q_1} (-q_0 + q_1 - q_1(1+z))}{H_0 (-1 + 2q_0 - 2q_1 + 2q_1(1+z))} \right) \quad (5.9)$$

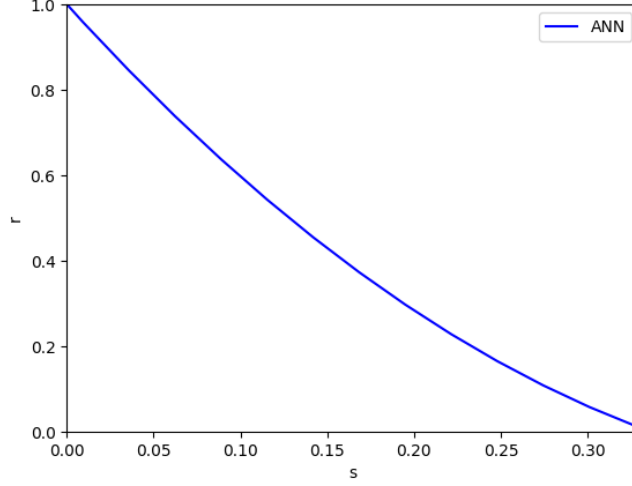


Figure 8: Illustrates the dynamics within the r - s plane of our model.

The statefinder diagnostics path is depicted in Figure 8. The development trajectory of our model concludes at the point $(r, s) = (1, 0)$ when $z = -1$, as illustrated in Eqs. (5.8) and (5.9). Consequently, our model aligns with the λ CDM model during the subsequent phases. The trajectory of the r - s parameter varies with the quintessence DE model and the Λ CDM model, as shown in Fig. 8, which further substantiates the hypothesis that the universe underwent multiple phases during its rapid expansion.

5.0.5 Energy Conditions

The physical violability of a structure is determined by its energy bonds. Null, weak, dominant, and strong energy states are widely recognized.

- $WEC = 36e^{4q_1 z} H_0^4 (1+z)^{4+4q_0-4q_1} - 3e^{2q_1 z} H_0^2 (1+z)^{2+2q_0-2q_1}$
- $NEC = 12e^{3q_1 z} H_0^3 (1+z)^{3+3q_0-4q_1} \left(e^{q_1 z} H_0 (1+z)^{1+q_0} + 2(1+z)^{q_1} \right) (1+q_0 - q_1 + q_1(1+z))$
- $DEC = D_1 \left[-(1+z)^{2q_1} - 2e^{2q_1 z} H_0^2 (1+z)^{2+2q_0} (-5 + q_0 - q_1 + q_1(1+z)) \right] -$

- $DEC = D_1 \left[-(1+z)^{2q_1} - 2e^{2q_1z} H_0^2 (1+z)^{2+2q_0} (-5 + q_0 - q_1 + q_1(1+z)) \right] -$
- $SEC = S_1 \left[(1+z)^{2q_1} + 6e^{2q_1z} H_0^2 (1+z)^{2+2q_0} (-1 + q_0 - q_1 + q_1(1+z)) + 12e^{q_1z} H_0 (1+z)^{1+q_0+q_1} (1 + q_0 - q_1 + q_1(1+z)) \right]$

where $D_1 = 6e^{2q_1z} H_0^2 (1+z)^{2+2q_0-4q_1}$ & $S_1 = 6e^{2q_1z} H_0^2 (1+z)^{2+2q_0-4q_1}$.

This allows us to test the feasibility of our models in the presence of overhead energy use. In addition, it will help us depict the universe more precisely in our minds. The previous string of energy conditions is obtained by applying equations (5.1) and (5.0.1).

The figures presented in 9 illustrate the behavior of the current cosmological model under conditions of Null, Dominant, and Strong energy, accompanied by the appropriate selection of constants. Figure 9 illustrates that we have established $\rho \geq 0, \rho + p \geq 0$ and $\rho - p \geq 0$, indicating that our model successfully meets the criteria for the WEC, NEC, and DEC tests; however, it does not satisfy the SEC test. The universe's acceleration is substantiated by the breach of the Strong Energy Condition, which ensures the anti-gravitational effect induced by the non-metricity scalar of the universe [63].

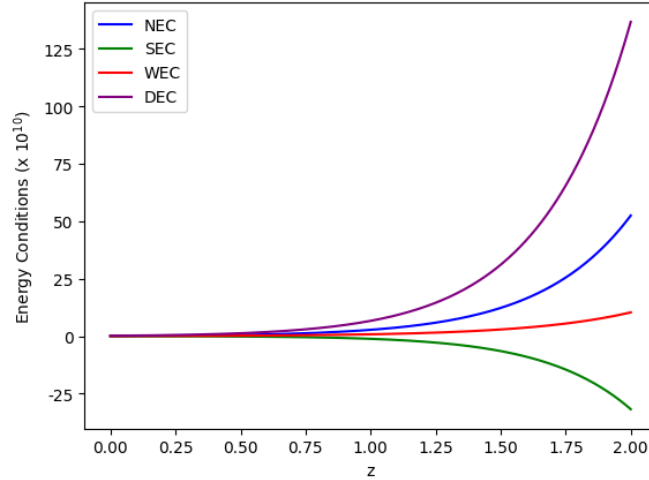


Figure 9: The energy conditions for the cubic $f(Q)$ gravity model are shown in the figure, along with their validity or non-validation.

5.1 Jerk Parameter

After the Hubble and deceleration parameters, the jerk parameter may reveal the universe's past. The jerk parameter, j , tracks the universe's acceleration with time. Positive j indicates acceleration and speeding up phase. However, when j is negative ($j \leq 0$), acceleration slows

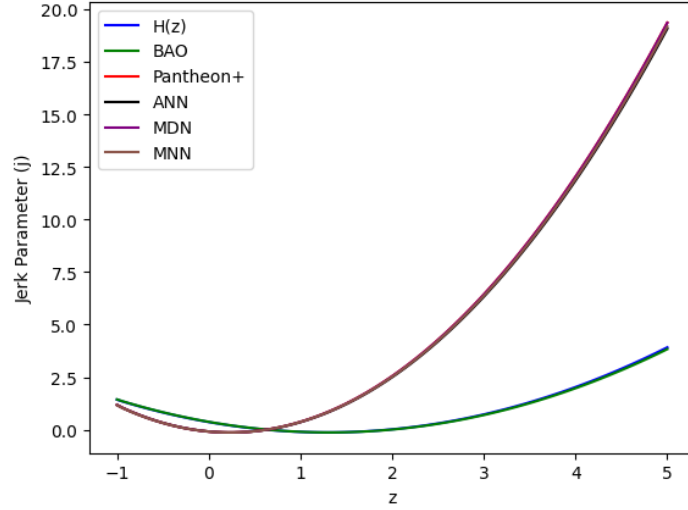


Figure 10: Graphical presentation of the jerk parameter vs redshift.

down. various dark energy theories predict various jerk parameters. By measuring j and comparing it to these predictions, scientists may learn more about dark energy.

Jerk Parameter is given by the equation;

$$j = \frac{\ddot{a}}{aH^3} \quad (5.10)$$

Also, the equation of the jerk parameter in terms of deceleration parameter q is given by;

$$j = q + 2q - \frac{\dot{q}}{H} \quad (5.11)$$

Thus, using Equation 5.5 we obtain jerk parameter as;

$$j = (1 + 2q_0 - 2q_1)(q_0 - q_1) - \frac{e^{-q_1 z} q_1 (1 + z)^{-1 - q_0 + q_1}}{H_0} + q_1 (1 + z) (1 + 4q_0 - 4q_1 + 2q_1 (1 + z)) \quad (5.12)$$

When combined with many other aspects of the universe, the jerk parameter makes a significant contribution to the enhancement of our models of the universe. These models are subjected to a stringent assessment in order to guarantee that they accurately mirror what we see in the actual universe. For the sake of this discussion, it is important to understand that Figure 10 illustrates the fluctuation of j in relation to redshift z for our model and the parameters that were obtained from it.

6 Concluding remarks

Through this research, we investigated the dynamics of a homogeneous, isotropic universe with cubic $f(Q)$ gravity. To do so, we used a simplified Hubble parameterization

Table 1: The values of the model's parameters that have been estimated.

Parameters	H_0 ($\text{km s}^{-1} \text{Mpc}^{-1}$)	q_0	q_1
OHD	$67.294^{+0.770}_{-0.455}$	$-0.748^{+0.061}_{-0.067}$	$0.384^{+0.033}_{-0.032}$
BAO	$67.567^{+0.677}_{-0.930}$	$-0.753^{+0.065}_{-0.058}$	$0.382^{+0.031}_{-0.032}$
Pantheon+	$69.969^{+0.390}_{-0.447}$	$-0.700^{+0.040}_{-0.039}$	$0.400^{+0.041}_{-0.039}$
ANN	$67.083^{+2.364}_{-2.871}$	$-0.403^{+0.132}_{-0.135}$	$0.655^{+0.110}_{-0.110}$
MDN	$67.076^{+3.018}_{-2.817}$	$-0.405^{+0.134}_{-0.137}$	$-0.651^{+0.115}_{-0.116}$
MNN	$67.032^{+2.843}_{-2.811}$	$-0.406^{+1.342}_{-1.337}$	$0.653^{+0.109}_{-0.118}$

of $H = H_0(1+z)^{1+q_0-q_1}e^{q_1z}$ to further investigate the dynamics of this universe. With the use of SN Ia observation data, we were able to constrain the free parameters of our model. Utilizing advanced Deep Learning techniques, the objective was to conduct an analysis of the rapid expansion of the universe and to estimate cosmological parameters simultaneously. CoLFI, which makes use of ANN, MDN, and MNN, performed an excellent job at estimating cosmological parameters. Because of this, it became much simpler to acquire knowledge about conditional probability densities based on observational data and posterior distributions. In order to increase the efficiency of neural network training and the accuracy of parameter predictions, hyperellipsoid parameters were implemented. After conducting a comparative research between our neural network approaches and the traditional MCMC methodology, we discovered that MNN gave findings that were virtually equivalent, demonstrating its suitability and trustworthiness.

The proposed universe model explains late time acceleration without dark energy and does not have cosmological constant issues. Given this, current observational data should be taken into account while simulating a $f(Q)$ gravity. We demonstrated that neural network approaches can estimate cosmological parameters, a viable MCMC alternative. The $f(Q)$ gravity framework allows for the investigation of different gravity theories and their effects on cosmic expansion using ANN, MDN, and MNN techniques. This is part of a machine learning-cosmology study. It shows how machine learning can handle complex cosmic dynamics and expansion problems. Since we evaluated density, cosmic pressure, equation of state, and deceleration parameters, our results are reliable.

References

- [1] G. Hinshaw *et al.* [WMAP], “First year Wilkinson Microwave Anisotropy Probe (WMAP) observations: The Angular power spectrum,” *Astrophys. J. Suppl.* **148** (2003), 135
- [2] G. Hinshaw *et al.* [WMAP], “Five-Year Wilkinson Microwave Anisotropy Probe (WMAP) Observations: Data Processing, Sky Maps, and Basic Results,” *Astrophys. J. Suppl.* **180** (2009), 225-245
- [3] G. Hinshaw *et al.* [WMAP], “Three-year Wilkinson Microwave Anisotropy Probe (WMAP) observations: temperature analysis,” *Astrophys. J. Suppl.* **170** (2007), 288
- [4] U. D. Goswami, “Supersymmetric hybrid inflation with non-minimal coupling to gravity,” *Eur. Phys. J. Plus* **135** (2020) no.1, 44
- [5] N. J. Cornish, D. N. Spergel, G. D. Starkman and E. Komatsu, “Constraining the topology of the universe,” *Phys. Rev. Lett.* **92** (2004), 201302
- [6] A. de Oliveira-Costa, M. Tegmark, M. Zaldarriaga and A. Hamilton, “The Significance of the largest scale CMB fluctuations in WMAP,” *Phys. Rev. D* **69** (2004), 063516
- [7] N. Schöneberg, L. Verde, H. Gil-Marín and S. Brieden, “BAO+BBN revisited — growing the Hubble tension with a 0.7 km/s/Mpc constraint,” *JCAP* **11** (2022), 039
- [8] S. Sanz-Wuhl, H. Gil-Marín, A. J. Cuesta and L. Verde, “BAO cosmology in non-spatially flat background geometry from BOSS+eBOSS and lessons for future surveys,” *JCAP* **05** (2024), 116
- [9] Verde, Licia, Nils Schöneberg, and Hector Gil-Marín. “A tale of many H 0.” *Annual Review of Astronomy and Astrophysics* 62 (2023).
- [10] Jimenez, Raul, Michele Moresco, Licia Verde, and Benjamin D. Wandelt. “Cosmic chronometers with photometry: a new path to H (z).” *Journal of Cosmology and Astroparticle Physics* 2023, no. 11 (2023): 047
- [11] L. K. Sharma, A. K. Yadav, P. K. Sahoo and B. K. Singh, “Non-minimal matter-geometry coupling in Bianchi I space-time,” *Results Phys.* **10**, 738-742 (2018)
- [12] A. K. Yadav, L. K. Sharma, B. K. Singh and P. K. Sahoo, “Existence of bulk viscous universe in $f(R, T)$ gravity and confrontation with observational data,” *New Astron.* **78**, 101382 (2020)
- [13] L. K. Sharma, A. K. Yadav and B. K. Singh, “Power-law solution for homogeneous and isotropic universe in $f(R, T)$ gravity,” *New Astron.* **79**, 101396 (2020)
- [14] L. K. Sharma, B. K. Singh and A. K. Yadav, “Viability of Bianchi type V universe in $f(R, T) = f_1(R) + f_2(R)f_3(T)$ gravity,” *Int. J. Geom. Meth. Mod. Phys.* **17**, no.07, 2050111 (2020)
- [15] L. K. Sharma, S. Parekh, S. Ray and A. K. Yadav, “Constraining anisotropic universe under $f(R, T)$ theory of gravity,” *JHEAp* **44** (2024), 457-467

- [16] S. Nojiri and S. D. Odintsov, "Unified cosmic history in modified gravity: from $F(R)$ theory to Lorentz non-invariant models," *Phys. Rept.* **505** (2011), 59-144
- [17] F. Esposito, S. Carloni, R. Cianci and S. Vignolo, "Reconstructing isotropic and anisotropic $f(Q)$ cosmologies," *Phys. Rev. D* **105** (2022) no.8, 084061
- [18] H. Amirhashchi and S. Amirhashchi, "Constraining Bianchi Type I Universe With Type Ia Supernova and $H(z)$ Data," *Phys. Dark Univ.* **29** (2020), 100557
- [19] H. Amirhashchi and S. Amirhashchi, "Recovering Λ CDM model from a cosmographic study," *Gen. Rel. Grav.* **52** (2020) no.2, 13
- [20] L. Tedesco, "Ellipsoidal Expansion of the Universe, Cosmic Shear, Acceleration and Jerk Parameter," *Eur. Phys. J. Plus* **133** (2018) no.5, 188
- [21] X. H. Ge and S. P. Kim, "An ellipsoidal universe in the brane world," *JCAP* **07** (2007), 001
- [22] L. Campanelli, P. Cea, G. L. Fogli and A. Marrone, "Testing the Isotropy of the Universe with Type Ia Supernovae," *Phys. Rev. D* **83** (2011), 103503
- [23] B. Mishra, G. Ribeiro and P. H. R. S. Moraes, "De Sitter and bounce solutions from anisotropy in extended gravity cosmology," *Mod. Phys. Lett. A* **34** (2019) no.39, 1950321
- [24] A. De, S. Mandal, J. T. Beh, T. H. Loo and P. K. Sahoo, "Isotropization of locally rotationally symmetric Bianchi-I universe in $f(Q)$ -gravity," *Eur. Phys. J. C* **82** (2022) no.1, 72
- [25] L. A. Devi, S. S. Singh, L. Kumrah and M. K. Alam, "Anisotropic solutions in $f(Q)$ gravity with hybrid expansion," *Z. Naturforsch. A* **78** (2023) no.7, 605-614
- [26] L. K. Sharma, S. Parekh, A. K. Yadav and N. Goyal, "A comprehensive analysis of observational cosmology in $f(Q)$ gravity with deep learning and MCMC method," *Astron. Comput.* **49** (2024), 100892
- [27] Team, The Theano Development, Rami Al-Rfou, Guillaume Alain, Amjad Almahairi, Christof Angermueller, Dzmitry Bahdanau, Nicolas Ballas et al. "Theano: A Python framework for fast computation of mathematical expressions." arXiv preprint arXiv:1605.02688 (2016).
- [28] P. Graff, F. Feroz, M. P. Hobson and A. Lasenby, "BAMBI: blind accelerated multimodal Bayesian inference," *Mon. Not. Roy. Astron. Soc.* **421** (2012), 169-180
- [29] A. Spurio Mancini, D. Piras, J. Alsing, B. Joachimi and M. P. Hobson, "CosmoPower: emulating cosmological power spectra for accelerated Bayesian inference from next-generation surveys," *Mon. Not. Roy. Astron. Soc.* **511** (2022) no.2, 1771-1788
- [30] J. d. Olvera, I. Gómez-Vargas and J. A. Vázquez, "Observational Cosmology with Artificial Neural Networks," *Universe* **8** (2022) no.2, 120
- [31] Escamilla-Rivera, Celia, Maryi A. Carvajal Quintero, and Salvatore Capozziello. "A deep

- learning approach to cosmological dark energy models." *Journal of Cosmology and Astroparticle Physics* 2020, no. 03 (2020): 008.
- [32] G. J. Wang, X. J. Ma, S. Y. Li and J. Q. Xia, "Reconstructing Functions and Estimating Parameters with Artificial Neural Networks: A Test with a Hubble Parameter and SNe Ia," *Astrophys. J. Suppl.* **246** (2020) no.1, 13
- [33] H. N. Lin, X. Li and L. Tang, "Non-parametric reconstruction of dark energy and cosmic expansion from the Pantheon compilation of type Ia supernovae," *Chin. Phys. C* **43** (2019) no.7, 075101
- [34] P. Graff, F. Feroz, M. P. Hobson and A. Lasenby, "BAMBI: blind accelerated multimodal Bayesian inference," *Mon. Not. Roy. Astron. Soc.* **421** (2012), 169-180
- [35] N. Perraudin, M. Defferrard, T. Kacprzak and R. Sgier, "DeepSphere: Efficient spherical Convolutional Neural Network with HEALPix sampling for cosmological applications," *Astron. Comput.* **27** (2019), 130-146
- [36] Ishida, Emille EO. "Machine learning and the future of supernova cosmology." *Nature Astronomy* 3, no. 8 (2019): 680-682.
- [37] Geman, Stuart, Elie Bienenstock, and RenÅ© Doursat. "Neural networks and the bias/variance dilemma." *Neural computation* 4, no. 1 (1992): 1-58.
- [38] S. Nojiri and S. D. Odintsov, "Unified cosmic history in modified gravity: from F(R) theory to Lorentz non-invariant models," *Phys. Rept.* **505** (2011), 59-144
- [39] S. Capozziello and R. D'Agostino, "Model-independent reconstruction of $f(Q)$ non-metric gravity," *Phys. Lett. B* **832** (2022), 137229
- [40] M. Moresco, A. Cimatti, R. Jimenez, L. Pozzetti, G. Zamorani, M. Bolzonella, J. Dunlop, F. Lamareille, M. Mignoli and H. Pearce, *et al.* "Improved constraints on the expansion rate of the Universe up to $z \sim 1.1$ from the spectroscopic evolution of cosmic chronometers," *JCAP* **08** (2012), 006
- [41] Moresco, Michele. "Raising the bar: new constraints on the Hubble parameter with cosmic chronometers at $z \sim 2$." *Monthly Notices of the Royal Astronomical Society: Letters* 450, no. 1 (2015): L16-L20.
- [42] Moresco, Michele, Lucia Pozzetti, Andrea Cimatti, Raul Jimenez, Claudia Maraston, Licia Verde, Daniel Thomas, Annalisa Citro, Rita Tojeiro, and David Wilkinson. "A 6% measurement of the Hubble parameter at $z \sim 0.45$: direct evidence of the epoch of cosmic re-acceleration." *Journal of Cosmology and Astroparticle Physics* 2016, no. 05 (2016): 014.
- [43] A. K. Yadav et al., "Reconstructing $f(Q)$ gravity from parameterization of the Hubble parameter and observational constraints," *J. High Energy Astrophys.* **43** (2024), 114-125.

- [44] D. Brout, D. Scolnic, B. Popovic, A. G. Riess, J. Zuntz, R. Kessler, A. Carr, T. M. Davis, S. Hinton and D. Jones, *et al.* "The Pantheon+ Analysis: Cosmological Constraints," *Astrophys. J.* **938** (2022) no.2, 110
- [45] G. J. Wang, C. Cheng, Y. Z. Ma and J. Q. Xia, Likelihood-free Inference with the Mixture Density Network, *Astrophys. J. Supp.* **262** (2022) 24
- [46] G. J. Wang et al. CoLFI: Cosmological Likelihood-free Inference with Neural Density Estimators, *Astrophys. J. Suppl.* **268** (2023) 7
- [47] G. J. Wang, S. Y. Li and J. Q. Xia, ECoPANN: A Framework for Estimating Cosmological Parameters using Artificial Neural Networks, *Astrophys. J. Suppl.* **249** (2020) 25
- [48] Sharma, L. K., S. Parekh, A. K. Yadav, and N. Goyal. "A comprehensive analysis of observational cosmology in $f(Q)$ gravity with deep learning and MCMC method." *Astronomy and Computing* (2024): 100892.
- [49] L. Verde, T. Treu and A. G. Riess, "Tensions between the Early and the Late Universe," *Nature Astron.* **3** (2019), 891
- [50] Solanki, Raja, S. K. J. Pacif, Abhishek Parida, and P. K. Sahoo. "Cosmic acceleration with bulk viscosity in modified $f(Q)$ gravity." *Physics of the Dark Universe* **32** (2021): 100820.
- [51] Koussour, M., S. H. Shekh, and M. Bennai. "Cosmic acceleration and energy conditions in symmetric teleparallel $f(Q)$ gravity." *Journal of High Energy Astrophysics* **35** (2022): 43-51.
- [52] Koussour, M., S. H. Shekh, and M. Bennai. "Anisotropic nature of space-time in $f(Q)$ gravity." *Physics of the Dark Universe*, **36** (2022): 101051.
- [53] de Haro, Jaume, Shin'ichi Nojiri, Sergei D. Odintsov, Vasilis K. Oikonomou, and Supriya Pan. "Finite-time cosmological singularities and the possible fate of the Universe." *Physics Reports* **1034** (2023): 1-114.
- [54] Nojiri, Shin'ichi, and Sergei D. Odintsov. "Well-defined $f(Q)$ gravity, reconstruction of FLRW spacetime, and unification of inflation with the dark energy epoch." *Physics of the Dark Universe* **43** (2024): 101538.
- [55] Hu, Kun, Makishi Yamakoshi, Taishi Katsuragawa, Shin'ichi Nojiri, and Taotao Qiu. "Nonpropagating ghost in covariant $f(Q)$ gravity." *Physical Review D* **108**(12) (2023): 124030.
- [56] Capozziello, Salvatore, Maurizio Capriolo, and Shin'ichi Nojiri. "Gravitational waves in $f(Q)$ non-metric gravity via geodesic deviation." *Physics Letters B* **850** (2024): 138510.
- [57] Farooq, Omer, and Bharat Ratra. "Hubble parameter measurement constraints on the cosmological deceleration-acceleration transition redshift." *The Astrophysical Journal Letters*, **766**, no. 1 (2013): L7.
- [58] Cunha, Joao Vital. "Kinematic constraints to the transition redshift from supernovae type Ia

union data." *Physical Review D—Particles, Fields, Gravitation, and Cosmology*, **79**, no. 4 (2009): 047301.

- [59] Lu, Jianbo, Lixin Xu, and Molin Liu. "Constraints on kinematic models from the latest observational data." *Physics Letters B* 699, no. 4 (2011): 246-250.
- [60] Yang, Yingjie, and Yungui Gong. "The evidence of cosmic acceleration and observational constraints." *Journal of Cosmology and Astroparticle Physics* 2020, no. 06 (2020): 059.
- [61] Yadav, Anil Kumar, Avinash K. Yadav, Manvinder Singh, Rajendra Prasad, Nafis Ahmad, and Kangujam Priyokumar Singh. "Constraining a bulk viscous Bianchi type I dark energy dominated universe with recent observational data." *Physical Review D* 104, no. 6 (2021): 064044.
- [62] Capozziello, Salvatore, Rocco D'Agostino, and Orlando Luongo. "High-redshift cosmography: auxiliary variables versus Padé polynomials." *Monthly Notices of the Royal Astronomical Society* 494, no. 2 (2020): 2576-2590.
- [63] A. K. Yadav, "Transitioning Scenario of Bianchi-I Universe within $f(R, T)$ Formalism", *Braz. J. Phys.* **49** (2019) 262